Brazilian Journal of Physics (2022) 52: 105
https://doi.org/10.1007/s13538-022-01103-w

SOCIEDADE BRASILEIRA DE FÍSICA

CONDENSED MATTER

Structural, Optical, Spectral, Thermal and Third-order NLO Behaviour of 4-Chlorobenzhydrazide Trichloro Acetate Single Crystal

C. Arunagiri[1,2] · S. Selvakumar[1,2] · N. K. Lokanath[3]

Received: 19 September 2021 / Accepted: 1 April 2022 / Published online: 20 April 2022

Abstract
Hirshfeld surface analysis and molecular structure determination of 4-chlorobenzhydrazide trichloro acetate (4CBTCA) single crystals has been grown by the slow evaporation method at room temperature. The title compound was confirmed by single and powder X-ray diffraction studies. The determination of the single crystal structure establishes that the title compound associate with the triclinic system with the space group P $\overline{1}$. Powder XRD affirmed the crystalline nature of the crystal. The molecular structure and existence of the vibrations were revealed by NMR experiments. The identity of distinct functional groups of title of the compound was determined by FT-IR and FT-Raman spectral analyses. UV–Vis–NIR analysis was performed to examine the optical property of the grown crystal, and the maximum absorbance wavelength is realized at 390 nm. This study discusses the 4-chlorobenzhydrazide trichloro acetate crystal and demonstrates blue and green emissions at 440 and 544 nm. The thermal behaviour of the (4CBTCA) was studied by thermo-gravimetric analysis (TGA), differential thermal analysis (DTA) and differential scanning calorimetry (DSC). Third-order nonlinear refractive index and nonlinear absorption coefficient have been determined by the third-order NLO studies.

Keywords X-ray Diffraction · Optical · Thermal analysis · Hirshfeld surface analysis · Third-order nonlinear properties

1 Introduction

Recent years have seen a great deal of interest in the second- and third-order NLO materials owing to the broad range of applications they provide in the areas of molecular electronics, photonics, and optics computing [1–3]. Organic, inorganic and semi-organic products of NLO have been identified [4, 5]. Because of their flexibility, organic NLO materials are commonly used. Because of their easy coordination, low costs and a lot of possible NLO materials, organic materials are popular [6, 7]. Schiff base is one of the best methods for synthesis of organic NLO materials. Generally, Schiff base is synthesized from simple condensation method by treating with an aldehyde and aromatic primary amines. Hydrazide is an aromatic aldehyde which has a variety of applications such as second harmonic generation (SHG), optoelectronic, photocatalytic, photovoltaic, and optical information [8–10]. 4-chloro benzhydrazide is an acid hydrazide group. It has a wide application such as nonlinear optics, sensors, transistors, radars and rectifier [11, 12]. Most of researchers are offer a noticeable attention to grow organic single crystals for technological and to biological applications [13]. During the last few decades, hydrazide derivatives have gained greater attention in biological activities such as antibacterial [14, 15], antimicrobial [16–20], antifungal [21, 22], anti-tuberculosis [23–25], anticancer, anti-inflammatory and analgesic impact [26]. For this intention, many medicinal chemists have synthesized different hydrazide derivatives to investigate their biological activities. Antimicrobial behaviour in the scientific world is one of many biological properties. Organic single-crystal amino acids are playing an increasingly important role as strongly ordered nonlinear second-order optical materials [27, 28]. General experiments have been conducted on organic materials accommodate systems with several advantages in hydrazide. The fundamental organic structure of NLO

✉ C. Arunagiri
pevrarunphyics@gmail.com

1 PG & Research Department of Physics, Thanthai Periyar Government Arts and Science College (Autonomous), Tiruchirappalli 620 023, Tamil Nadu, India

2 Bharathidasan University, Tiruchirappalli 620 024, Tamil Nadu, India

3 Department of Physics, University of Mysore, Mysore 570 006, India

materials is based on the bond system; owing to the overlap of *p* orbitals, the relocation of electronic charge distribution leads to a high mobility of electrons. Functionalization of both ends of the bonding system with an effective electron donor and acceptor groups can further improve asymmetric electronic distribution in one or both ground and excited states, leading to an increased optical nonlinearity [29]. In particular, the effective delocalization of the *p* bond electrons was its foundation of the organic molecules, which contributes to the synthesis of molecular polarization. In general, high hyperpolarizability is the product of an appropriate combination of different aspects such as *p* bond, donor–acceptor categories, dimensionality and inclination for a certain crystal structure [30].

Organic materials-based single crystal form would be extremely interesting. Several studies have been reported on hydrazide [31] and trichloroacetic acid-based compounds, 2-aminopyridinium trichloro acetate [32], 3-nitroanilinium trichloro acetate [33], melaminium bis (trichloro acetate) [34] guanidine with acetic, trichloroacetic and trifluoroacetic acids [35] and guanidinium trichloro acetate [36–38], respectively. Accordingly, the slow evaporation method is acquired to grow this crystal. In this present study, 4-chlorobenzhydrazide trichloroacetic acid single (4CBTCA) crystal was successfully grown with an equimolar ratio by the slow evaporation method which has still not been published and the grown crystal was analysed by single crystal X-ray diffraction study, powder XRD, spectral studies, third harmonic generation analysis, fluorescence and thermal behaviour.

2 Material Synthesis and Crystal Growth

4-chlorobenzhydrazide trichloro acetate (4CBTCA) salt was synthesized with an equimolar ratio of 1:1 at ambient temperature by dissolving mixed solvents of AR grade 4-chlorobenzhydrazide (Sigma Aldrich, 99 percent) and trichloroacetic acid (Merck, 99.5 percent). A magnetic stirrer was utilized to achieve a homogeneous solution; the resulting solution was well stirred for 3 h, where after solution was filtered and ideally placed at ambient temperature evaporation. After complete evaporation, the salts were collected.

4CBTCA single crystal was grown by solution growth technique using synthesized materials. The saturated solution was prepared at room temperature and stirred continuously for 2 h. After that, the able solution was filtered by Whatman filter paper into a beaker and covered with perforated aluminium foil cover to control the rapid evaporation of the mixed solvent. After 11 days, white-coloured needles like single crystals of dimension around $5 \times 3 \times 2$ mm^3 were gathered. The 4CBTCA single crystals are shown in Fig. 1.

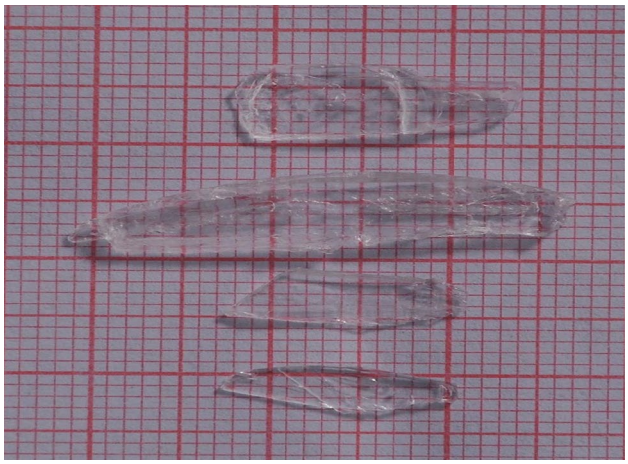

Fig. 1 Grown 4CBTCA single crystals

3 Results and Discussion

3.1 Single Crystal X-ray Diffraction Analysis

Single crystal X-ray diffraction analysis of 4CBTCA crystal was carried out using BRUKER AXES KAPPA APEX2 CCD diffractometer with a MoKα (0.71073 Å) radiation to determine the molecular structure and to estimate the lattice parameter values. The crystal structure was resolved by the direct method and refined by the full matrix least square technique using the SHELXL program. Least squares refinement of 165 reflections was performed in the range of 20–30°. The single crystal X-ray analysis confirmed that the as-grown 4CBTCA crystal belongs to the triclinic system with the centrosymmetric space group P $\bar{1}$ and the obtained cell parameters are $a = 5.826(3)$ Å, $b = 9.253$ (4) Å, $c = 12.908$ (6) Å, $\alpha = 97.354$ (9)°, $\beta = 100.629$ (9)°, $\gamma = 91.245$ (8)° and $V = 677.6$ (5) Å^3. 4CBTCA cell parameters obtained from this study shown in Table 1 and the crystal structure with atomic-numbering are shown in Fig. 2.

It consists of one 4-chlorobenzhydrazide cations and one trichloro acetate anion. The protonated planner of 4-chlorobenzhydrazide in 4CBTCA molecules gateway is the cation with a positively charged amine group, whereas the trichloroacetic acid is in the anionic state. The 4- chlorobenzhydrazide cations and trichloro acetate anions are linked together by an inestimable network of hydrogen bonds. The final fractional position coordinates with equivalent isotropic and anisotropic temperature factors for all non-hydrogen atoms are given in Tables 2 & 3.

Atoms C12 – N11 – N8 and O2 – C12 – N11 participate in the hydrogen bonding network as both acceptor and donors, mediating the amine and acid interactions. The bond lengths and angles of non-hydrogen atoms of

Table 1 Crystal data and structure refinement details for 4CBTCA single crystal

CCDC deposit No	2,051,383
Moiety formula	$C_7H_7ClN_2O$, $C_2Cl_3O_2$
Crystal data Formula	$C_9H_7Cl_4N_2O_3$
Formula weight	332.97
Crystal system	Triclinic
Space group	P $\bar{1}$
a, b, c [Å]	5.826 (3), 9.253 (4), 12.908 (6)
α, β, ν [˚]	97.354 (9), 100.629 (9), 91.245 (8)
V[Å^3]	677.6 (5)
Z	2
D(calc)[Mg/m^3]	1.632
μ(Mo Kα) [/mm^{-1}]	0.873
F(000)	334.0
Crystal size [mm^3]	0.30×0.25×0.20
θ Min–Max [˚]	3.24–27.38
Dataset	−7→7: −11→10: −16→15
Temperature (K)	293
Radiation [Å]	MoKα 0.71075
Nref, Npar	2987,165
R, wR2, S	0.0568, 0.1534, 1.023
H-atom treatment	H-atom parameters constrained
Largest diff. peak and hole (e/Å^{-3})	0.531, −0.462

Table 2 Fractional atomic coordinates and isotropic or equivalent isotropic displacement parameters (Å^2) of 4CBTCA single crystal

Atoms	*X*	*Y*	*Z*	U_{iso}*/U_{eq}
Cl2	1.1098 (2)	0.27199 (9)	0.15902 (9)	0.0758 (4)
Cl3	1.27742 (19)	0.50878 (16)	0.32261 (8)	0.0843 (4)
Cl4	1.2922 (2)	0.24337 (13)	0.54577 (8)	0.0817 (4)
O5	1.2947 (4)	0.4927 (2)	0.05711 (18)	0.0445 (6)
O6	1.1192 (4)	0.6825 (2)	0.12405 (19)	0.0461 (6)
O7	0.4634 (4)	0.0143 (2)	0.11938 (18)	0.0433 (5)
N8	0.5235 (4)	−0.2393 (2)	0.0179 (2)	0.0381 (6)
H8A	0.5790	−0.3158	−0.0135	0.046*
H8B	0.3912	−0.2645	0.0338	0.046*
C9	1.1733 (4)	0.5532 (3)	0.1172 (2)	0.0297 (6)
C10	1.0891 (5)	0.4602 (3)	0.1982 (2)	0.0356 (6)
N11	0.6832 (4)	−0.1811 (2)	0.1120 (2)	0.0398 (6)
H11	0.8020	−0.2276	0.1376	0.048*
C12	0.6373 (5)	−0.0479 (3)	0.1589 (2)	0.0336 (6)
C13	1.1703 (6)	0.0307 (4)	0.3801 (3)	0.0516 (8)
H13	1.3166	−0.0051	0.4023	0.062*
C14	0.7350 (6)	0.1406 (3)	0.3153 (3)	0.0453 (8)
H14	0.5895	0.1777	0.2935	0.054*
C15	0.8016 (5)	0.0156 (3)	0.2568 (2)	0.0360 (7)
C16	0.8824 (7)	0.2092 (4)	0.4050 (3)	0.0535 (9)
H16	0.8366	0.2914	0.4442	0.064*
C17	1.0207 (6)	−0.0386 (3)	0.2911 (3)	0.0453 (8)
H17	1.0663	−0.1223	0.2536	0.054*
C18	1.0994 (7)	0.1539 (4)	0.4355 (3)	0.0513 (8)
Cl1	0.79822 (14)	0.49307 (10)	0.21161 (8)	0.0565 (3)

the title crystal are obtained (Table 4). The two rings of 4CBTCA cations approximately co-planer crystallographic *ab* axis. All hydrogen atoms protonated amine group mixed up in N–H●●●O hydrogen bonds with near trichloro acetate anions. The hydrogen coordinates and

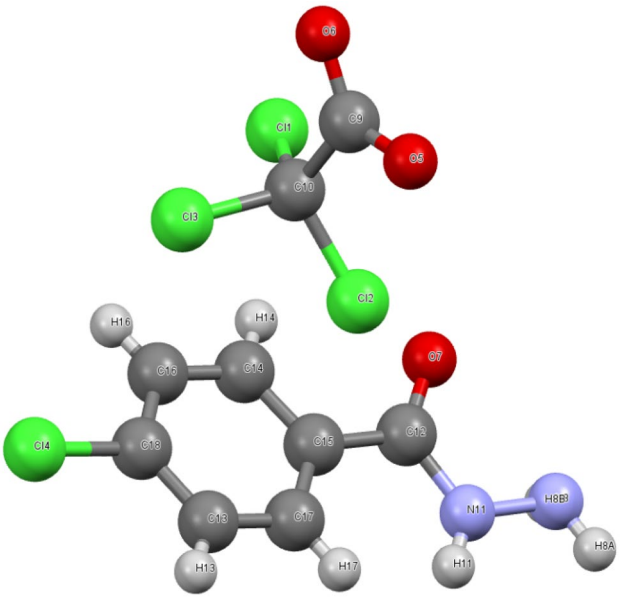

Fig. 2 ORTEP of grown 4CBTCA single crystal

equivalent isotropic distance H8A and H8B (0.046), H11 (0.048), H13(0.062), H14 and H17 (0.054). Atoms C12 – N11 – N8 and O2 – C12 – N11 go in for in the hydrogen bonding network as both acceptor and donors, mediating the amine and acid interactions.

All hydrogen atoms protonated amine group involved in N – H●●●O hydrogen bonds with near trichloro acetate anions. *ORTEP* of 4CBTCA is shown in Fig. 2, and the packing diagram is displayed in Fig. 3. Selected bond distances and angles are given in Table 4. The C12 - – C10 bond distance is 1.764 (3)˚A which is characteristic of the C — – C bond. The observed dihedral angle between the O7 and N11 is 119.5 (3) ° [O7-C12-N11]. From the geometrical parameters, it is observed that the 4-chlorobenzhydrazide with trichloro acetate atoms participating in the hydrogen bonding network N11-C12 — – C15 and N8 — – N11 is 1.423(3). The observed O5 — – C9 bond distance is 1.235(3), O6 — – C9 (1.240(3)), C9 — – C10 (1.574(4)), C15 — – C17 (1.398(4)) and C13—C18 bond distances are presented in Table 4. The atomic displacement parameters are C13 (-0.0026), N8 (0.0007), N11 (0.0025), O5 (0.074), O6 (0.0088) in U[23] modify. In the 4CBTCA, the hydrogen group forms an intra-molecular N8 — – H8*A*●●●O5^{i}

Table 3 Atomic displacement parameters (Å^2) of 4CBTCA single crystal

Atoms	U_{11}	U_{22}	U_{33}	U_{12}	U_{13}	U_{23}
Cl2	0.1140 (9)	0.0337 (4)	0.1054 (9)	0.0184 (5)	0.0737 (7)	0.0267 (5)
Cl3	0.0579 (6)	0.1474 (12)	0.0434 (5)	−0.0159 (7)	−0.0043 (4)	0.0206 (6)
Cl4	0.0928 (9)	0.0914 (8)	0.0503 (6)	−0.0222 (7)	0.0005 (5)	−0.0064 (5)
O5	0.0492 (12)	0.0323 (10)	0.0607 (14)	0.0069 (10)	0.0283 (11)	0.0117 (10)
O6	0.0466 (13)	0.0272 (10)	0.0677 (15)	0.0078 (9)	0.0176 (11)	0.0074 (10)
O7	0.0445 (12)	0.0339 (10)	0.0537 (13)	0.0155 (9)	0.0109 (10)	0.0088 (9)
N8	0.0379 (13)	0.0273 (12)	0.0499 (15)	0.0006 (10)	0.0135 (12)	0.0007 (11)
C9	0.0225 (12)	0.0276 (13)	0.0371 (14)	−0.0018(10)	0.0012 (11)	0.0038 (11)
C10	0.0331 (14)	0.0363 (14)	0.0403 (16)	0.0094 (12)	0.0119 (12)	0.0078 (12)
N11	0.0387 (14)	0.0266 (12)	0.0508 (15)	0.0100 (11)	0.0012 (12)	0.0025 (11)
C12	0.0379 (15)	0.0260 (13)	0.0429 (16)	0.0047 (12)	0.0189 (13)	0.0099 (12)
C13	0.0486 (19)	0.0524 (19)	0.054 (2)	0.0024 (16)	0.0077 (16)	0.0089 (16)
C14	0.0499 (19)	0.0414 (16)	0.0479 (19)	0.0054 (15)	0.0194 (15)	0.0030 (14)
C15	0.0400 (16)	0.0293 (13)	0.0426 (16)	0.0012 (12)	0.0154 (13)	0.0091 (12)
C16	0.067 (2)	0.0468 (18)	0.049 (2)	−0.0030(18)	0.0241 (18)	−0.0035 (16)
C17	0.0474 (18)	0.0372 (16)	0.0522 (19)	0.0080 (14)	0.0113 (15)	0.0060 (14)
C18	0.060 (2)	0.057 (2)	0.0369 (17)	−0.0133(17)	0.0084 (15)	0.0070 (15)
Cl1	0.0339 (4)	0.0651 (6)	0.0810 (7)	0.0138 (4)	0.0241 (4)	0.0282 (5)

$(-x+2,-y,-z)$, N8 — – H8*B*●●●O6^{ii} (x − 1, $y-1$, z;) and C17 — – H17 ··· ●●● O6^{iii} (x, $y-1$, z of hydrazide with acid fragments (Table 5).

Table 4 Selected geometric parameters of 4CBTCA single crystal

Bond lengths (Å)			
Cl2—C10	1.764 (3)	N11—C12	1.357 (3)
Cl3—C10	1.768 (3)	C12—C15	1.482 (4)
Cl4—C18	1.744 (4)	C13—C18	1.379 (5)
O5—C9	1.235 (3)	C13—C17	1.382 (5)
O6—C9	1.240 (3)	C14—C16	1.379 (5)
O7—C12	1.236 (3)	C14—C15	1.401 (4)
N8—N11	1.423 (3)	C15—C17	1.398 (4)
C9—C10	1.574 (4)	C16—C18	1.383 (5)
C10—Cl1	1.764 (3)		
Bond angles (°)			
O5—C9—O6	126.7 (3)	N11—C12—C15	117.3 (2)
O5—C9—C10	117.2 (2)	C18—C13—C17	119.0 (3)
O6—C9—C10	116.1 (2)	C16—C14—C15	120.8 (3)
C9—C10—Cl2	111.16 (19)	C17—C15—C14	118.7 (3)
C9—C10—Cl1	112.05 (18)	C17—C15—C12	123.8 (3)
Cl2—C10—Cl1	108.57 (17)	C14—C15—C12	117.4 (3)
C9—C10—Cl3	107.3 (2)	C14—C16—C18	118.8 (3)
Cl2—C10—Cl3	108.11 (15)	C13—C17—C15	120.7 (3)
Cl1—C10—Cl3	109.52 (16)	C13—C18—C16	121.9 (3)
C12—N11—N8	116.2 (2)	C13—C18—Cl4	118.7 (3)
O7—C12—N11	119.5 (3)	C16—C18—Cl4	119.4 (3)

3.2 Determination of Some Fundamental Data

The free electron plasma energy $\hbar\omega_P$ is considered as:

$$\hbar\omega_P = 28.8(Z\rho/M)^{1/2}$$

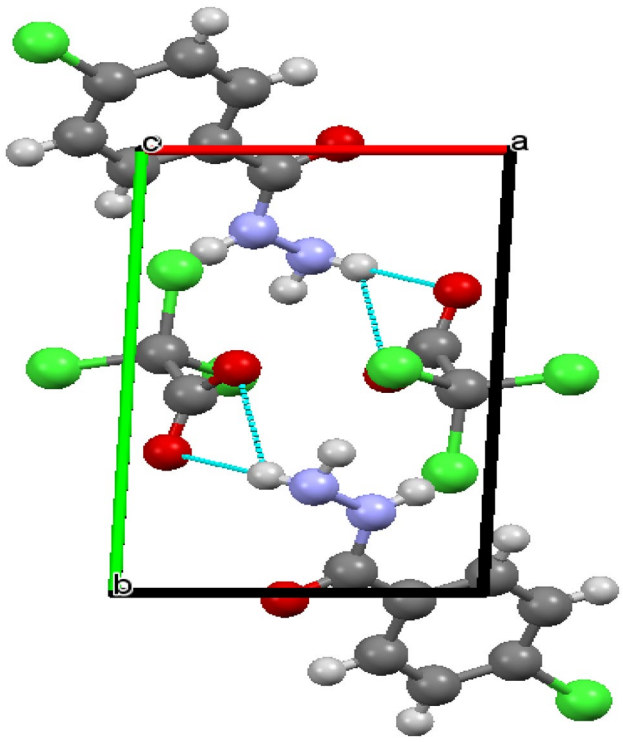

Fig. 3 Packing of the molecules when viewed down along ab axis of grown 4CBTCA single crystal

Table 5 Hydrogen-bond geometry (Å)

D—H···*A*	*D*—H	H···*A*	*D*···*A*	*D*—H···*A*
N8—H8*A*···O5^{i}	0.87	1.87	2.732 (3)	170
N8—H8*B*···O5^{ii}	0.87	2.37	2.934 (3)	123
N8—H8*B*···O6^{ii}	0.87	2.21	3.053 (4)	162
N11—H11···O6^{iii}	0.86	2.07	2.848 (4)	150
C17—H17···O6^{iii}	0.93	2.37	3.276 (4)	166

Symmetry codes: (i) $-x+2, -y, -z$; (ii) $x-1, y-1, z$; (iii) $x, y-1, z$

where ρ is the density, Z is the total number of free electron, and M is the molecular weight of the crystal. The Fermi energy and Penn gap are obviously dependent on the $\hbar\omega_P$ [39]. The Penn gap energy is calculated using the relation.

$$E_P = \frac{\hbar\omega_P}{(\varepsilon_\infty - 1)^{1/2}}$$

The Fermi energy is established from the relation: $E_F = 0.2948(\omega_P)^{4/3}$ Polarizability α was attained by using the following relation [40]:

$$\alpha = \left[\frac{(\hbar\omega_P)^2 S_0}{(\hbar\omega_P)^2 S_0 + 3E_P{}^2}\right] + \frac{M}{\rho} \times 0.396 \times 10^{-2} cm^{-3}$$

where S_0 is a constant for the material, which is given by

$$S_0 = 1 - \left[\frac{E_P}{4E_F}\right] + \frac{1}{3}\left[\frac{E_P}{4E_F}\right]^2$$

The value of α so obtained agrees well with that of Clausius–Mossotti equation, which is given by

$$\alpha = \frac{3M}{4\pi N_a \rho}\left(\frac{\varepsilon_\infty - 1}{\varepsilon_\infty + 2}\right)$$

The calculated data for the grown 4CBTCA crystal are presented in Table 6.

3.3 Hirshfeld Surface Analysis

It is influential to acquire quantitative evaluation of intermolecular interactions in the purpose of gaining a greater interpretation of intermolecular interactions in supramolecular assemblies. Hirshfeld surface analysis (HS) is potential to be a possible method for quantitatively explaining molecular crystal structures. Depending on the results of single crystal X-ray diffraction studies, Hirshfeld surface and 2D fingerprint plots were created using *Crystal Explorer* 3.1 [41–44]. The d_{norm} function is a proportion that involves the intervals linking the same surface point and the nearest interior (d_i) and exterior (d_e) atoms, and also the atoms' van der Waals radii [44]. The intermolecular low or huge contacts within the molecular structure can be identified using the molecular Hirshfeld surface analysis. Figure 4 depicts fingerprint plots (2D) revealing the percentage of area occupied by several types of intermolecular interactions. Figure 5(a) depicts the shape index d_{norm} and curvedness of the 4CBTCA molecule. The normalized contact distance d_{norm} based on the distance from a point on the surface to the nearest nucleus outside the surface di enables the identification of the regions of particular importance to the intermolecular interactions. The combination of d_e and d_i in the form of 2D fingerprint plot is shown in Fig. 5(b) which gives the summary of intermolecular contacts in the crystal lattice. The fingerprint plots reveal the ratio contribution of intermolecular performance to the surface which can be described in terms of colour codes. In the 4CBTCA, the addition owing to C●●●C interactions to the Hirshfeld surface is (19.1%) and that of C●●●H contacts [44] to the total Hirshfeld surface is (5.1%), while the C●●●Cl less behaviour contributing to third most Hirshfeld surface is 3.6% and the other intermolecular performance Cl●●●Cl (10.2%), Cl●●●H (30.9%), O●●●H (4.4%), Cl●●●N (1%), H●●●H (7.2%), Cl●●●O (6.6%), C●●●O (2%), O●●●H (24.8) and O●●●O (2%) for interactions for in for 4-chlorobenzhydrazide trichloro acetate. The intense red colour circular point revealed the intermolecular short contacts due to the showing of Cl●●●O hydrogen bonds. The sharp spikes in the fingerprint plot reveal the owing of Cl●●●Cl hydrogen bonds in the crystal structure of the 4CBTCA.

Table 6 Characteristic data of the 4CBTCA single crystal

Parameters	4CBTCA
Plasma energy (eV)	14.3
Penn gap (eV)	1.2223
S_0	3.922
Electronic Polarizability (Penn analysis) cm^3	4.4279×10^{-23}
Electronic Polarizability (Clausius Mossotti) cm^3	5.713×10^{-23}

3.4 Powder X-ray Diffraction Studies

The freshly crushed 4CBTCA powder of the crystal has been described by powder X-ray diffraction analysis using BRUKER X-ray diffraction with CuKα radiation of λ = 1.5406 Å. The 4CBTCA crystal was scanned in the range 10–70° at the rate of 1°min^{-1}. The evidence of powder X-ray diffraction pattern of 4CBTCA is depicted in Fig. 6, and the sharp peaks at specific 2θ values show high crystalline nature of the 4CBTCA crystals.

3.5 FT-IR and FT-Raman Spectral Studies

The Fourier transform infrared spectrum of the title crystal was recorded on a BRUKER IFS–66 V spectrophotometer

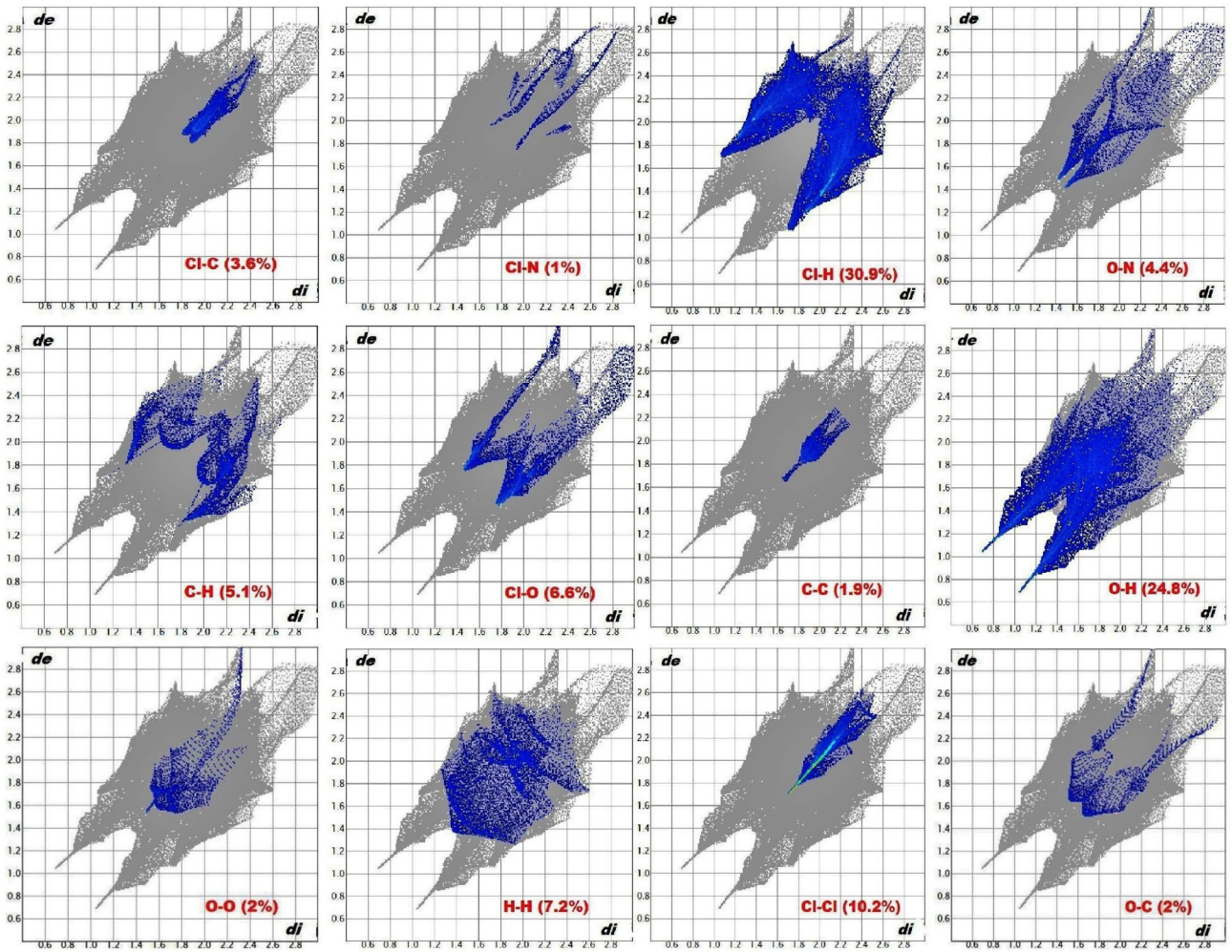

Fig. 4 2D-fingerprint plot of 4CBTCA

in the frequency range of 4000–400 cm^{-1} at a resolution of ± 1 cm^{-1} by using KBr pellet. Fourier Transform Raman spectrum has also been reported by the BRUKER KFS 27 FT-Raman spectrometer in the wavelength range of 50–4000 cm^{-1}. The presence of various functional groups is tabulated (Table 7) from the FT-IR and FT-Raman spectrum which is seen in Figs. 7 and 8, respectively. In the higher energy field, NH asymmetrical and symmetrical stretching is assigned to the specific characteristics observed at 3187 and 3036 cm^{-1}. The high absorption at 1651 cm^{-1} led to the identification of the amide (>C=O). This confirms the molecular structure of the material. The 750 and 668 cm^{-1} bands proved the presence of OH plane deformation in FT–IR and FT–Raman spectrum [35]. The CH_2 wagging vibration owes a sharp, intense peak at 1326 cm^{-1} in the FT–IR and FT–Raman spectra, respectively. The bands at 1190, 1094 and 1012 cm^{-1} recognized the presence of C–C stretching. The strong band observed at 836 cm^{-1} is due to the asymmetric stretching vibrations of C–Cl_3 in the FT–Raman spectrum. The band at 1260 cm^{-1} revealed the presence of C–H bending. The bands at 948 and 668 cm^{-1} illustrate the presence of CH_2 rocking vibration [45]. The C–C and C–CO deformation vibrations of 4CBTCA give their characteristic vibration at 580 and 521 cm^{-1}, respectively. The presence of COO^- rocking is clearly demonstrated by the peak at about 459 cm^{-1} in the title crystal. The peak at 1654 cm^{-1} is due to the presence of stretching vibration of COO^-, and the peak at 1596 cm^{-1} represents the bending vibrations of the N–H group [45]. The strong peak observed at 730 and 753 cm^{-1} corresponds to the in-plane deformation modes of COO^- group derived from trichloroacetic ions.

3.6 Nuclear Magnetic Resonance Spectroscopy

^1H NMR and ^{13}C NMR spectra were recorded on a 500 MHz AVANCE II (Bruker) spectrophotometer in deuterium oxide solvent. Hydrogen atoms involved in different regulatory

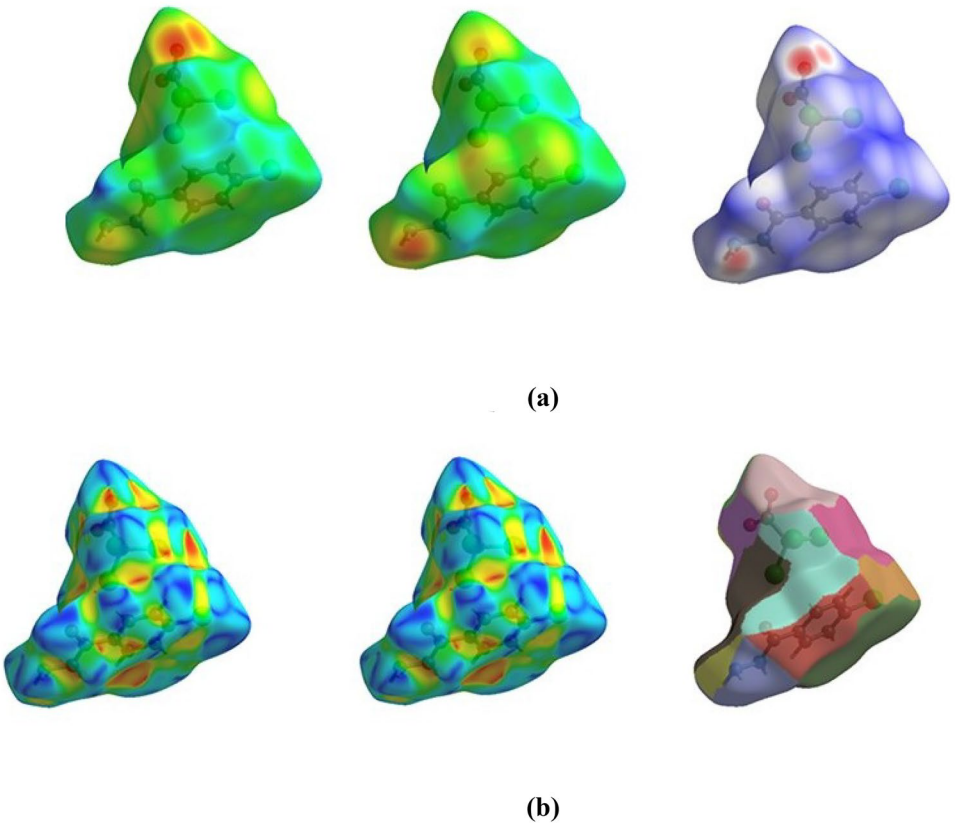

Fig. 5 **a** Hirshfeld surface de di dnorm of the 4CBTCH molecule **b** Curvedness, shape index and fragment patch of the 4CBTCH molecule

quality have been represented at different chemical shift positions. Since the compound involves different functional groups of hydrogen atoms 4-chlorobenzhydrazide trichloro acetate, the spectrum shows numerous signals at distinct δ positions. Hydrogen contained in 4–chlorobenzhydrazide can be seen positioned parallel to antiparallel resonance three to four times. Thus, the hydrogen appears as distorted multiple signals at 9.983 – 10.310 ppm (m, NH) and 8.327 – 7.529 ppm (m,

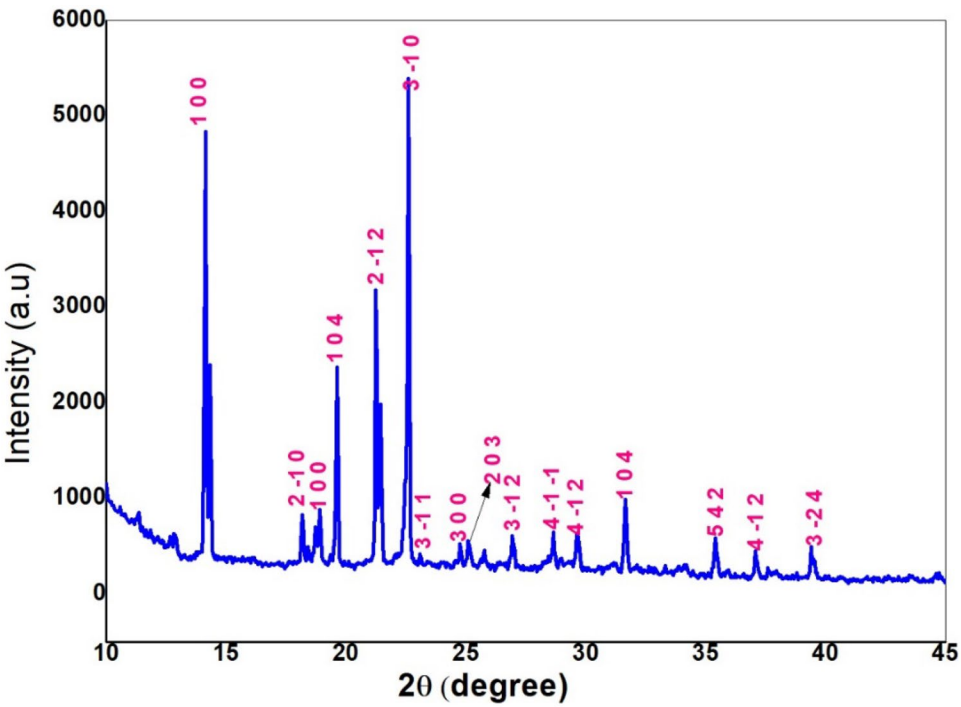

Fig. 6 Powder X-ray diffraction of grown 4CBTCA single crystal

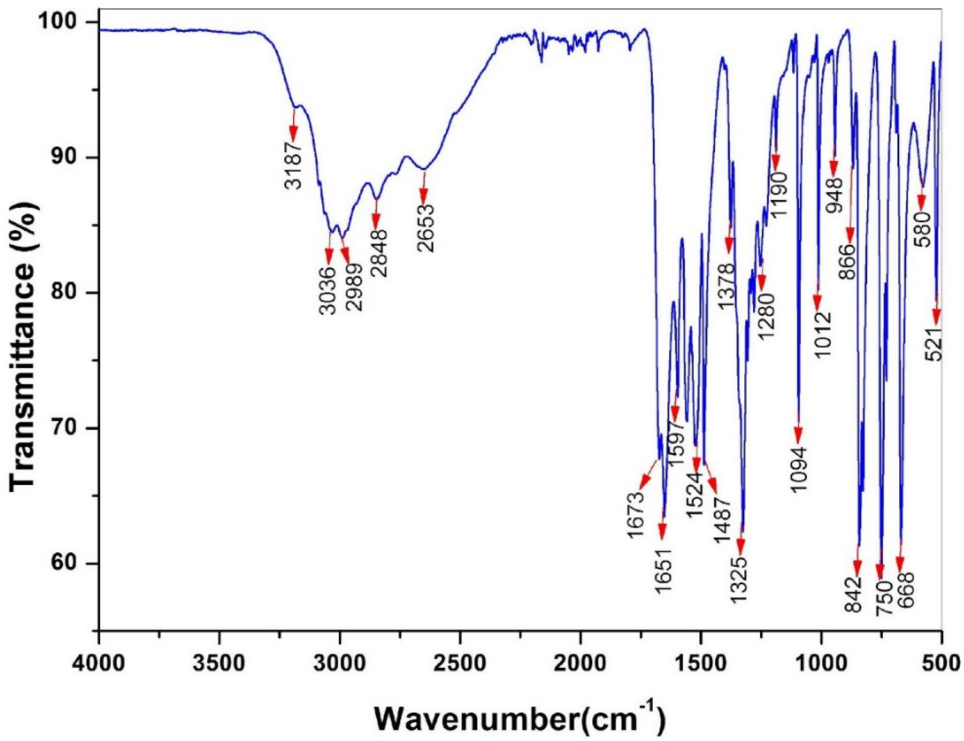

Fig. 7 FT-IR Spectrum of 4CBTCA single crystal

Ar–H) as shown in Fig. 9(a). In ^{13}C NMR spectrum, 165.26, 136.52–124.67, 79.65 and 40.60 – 39.35 ppm carbon groups are presented for the grown 4-chlorobenzhydrazide trichloro acetate single crystal depicted in Fig. 9(b).

3.7 UV–Vis-NIR Spectroscopy

The UV–Vis-NIR spectrum was measured for the 4CBTCA crystals by Varian carry 5000 UV–Vis-NIR spectroscopies.

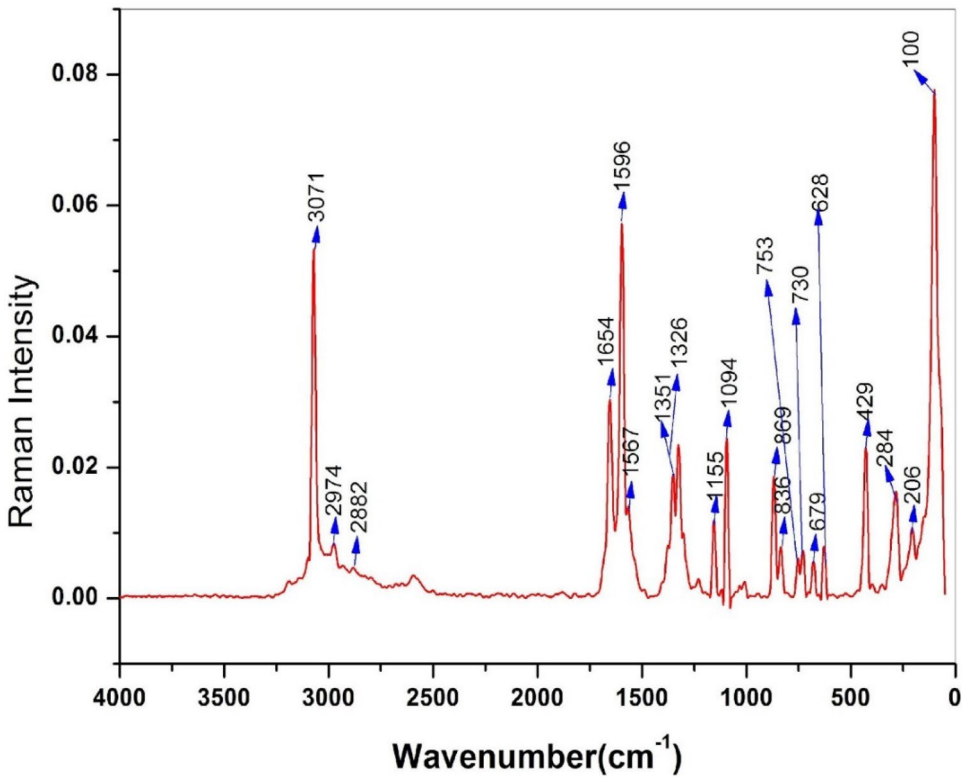

Fig. 8 FT-Raman Spectrum of 4CBTCA single crystal

Table 7 Vibrational band assignments of 4CBTCA single crystal

Wave number (in cm^{-1})		Assignments	Wave number (in cm^{-1})		Assignments
FT-IR	FT-Raman		FT-IR	FT-Raman	
3187	-	NH asymmetric stretching	1260	-	NH_3^+ deformation
-	3071	NH symmetric stretching	1094	1094	C– C stretching
3036	-	C–N out plane bending	1012	-	C– C stretching
2989	2974	Combination and overtone	948	-	C-NH stretching
2848	2882	CH_2 stretching	866	869	COO^-symmetric stretching
2663	-	C–H stretching	842	836	C–Cl_3asymmetricstretching vibrations
1673	-	C–H stretching	750	753	COO- in plane deformation
1651	1654	COO^- stretching vibration	668	679	NH_2 twisting
1624	-	O–H stretching	580	628	C–N bending
1597	1596	C– N ring stretching	521	-	C–N bending
-	1567	C–N stretching vibration	459	-	CCO deformation
1378	-	Ring: Semi-circle stretching	-	284	C–Cl_3 asymmetric deformation
-	1351	C–N stretching	-	206	C– Cl_3 rocking vibration
1326	1326	C– N semicircular ring	-	100	Lattice vibration

The absorption and transmittance spectrum of the grown 4CBTCA crystal is shown in Fig. 10. 4CBTCA crystal cut and polished with 2 mm thickness was used for the optical studies. It is observed that the cut-off wavelength is at 389 nm for the grown 4CBTCA single crystal. The 4CBTCA crystal is transparent through the entire visible region and the near IR region. It can be used as a window material for UV region. The majority of papers available in which UV–Vis—NIR spectroscopy has been used for the study of 4CBTCA crystal use the direct bandgap calculation, and the optical absorption coefficient can be determined from the maximum absorbance that used the ensuing formula as:

$$\alpha = \frac{1}{t} log\left(\frac{1}{T}\right)$$

$$\alpha = \frac{A(\mathrm{h}\upsilon - Eg)^{1/2}}{\mathrm{h}\upsilon}$$

where t is the sample thickness and $\log(\frac{1}{T})$ is defined as the absorbance of the sample. In the high photon energy region, the energy dependence of absorption coefficient (α) obeying the following relation for high proton energies (hυ) E_g is the optical band gap of the crystal and A is an optical constant. The variation of $(\alpha h\upsilon)^2$ versus hυ is plotted in Fig. 11, and E_g is evaluated by extrapolation of the linear part. The band gap is found to be 2.38 eV for the grown 4CBTCA single crystal.

3.8 Fluorescence Behaviour

The 4CBTCA crystal excitation and emission spectrum were reported in the F-7000 FL spectrophotometer. The spectrum of excitation was observed in the range of 200- 400 nm. The sample was excited at 274 nm. In Fig. 12, the emission spectrum was observed in the range from 400 to 700 nm. 4CBTCA crystal exhibits a green fluorescence property. The band gap energy was estimated using the formula:

$$E_g = \frac{hc}{\lambda} eV; E_g = \frac{1240}{\lambda} eV$$

The band gap energy correlates with the absorption maximum and can be approximately evaluated by the above relation, where *h* is the Planck's constant (6.626×10^{-34}Js), E_g is the band gap energy (eV), *c*is the light velocity (3×10^8 m/s), and λ is the wavelength (nm). In the 4CBTCA single crystal, band gap energy is obtained at 2.82 eV, and the present study shows a band gap specifying their activity in the visible region of the spectrum. The fluorescence samples exhibit the green and blue emission; the crystal can be esteemed that the 4CBTCA crystal is a promise candidate for opto-electronic fluorescence applications.

3.9 Thermal Properties

Thermo-gravimetric analysis (TGA) and differential thermal gravimetric analysis (DTG) were performed using SDT Q600 V8.3 Build 101 thermal analyser at temperatures ranging from 25 °C to 1000 °C at a heating rate of 20 °C/min in the process of a nitrogen atmosphere in alumina crucible. The mass of 4.153 mg of the material was analysed. The thermogram of the title compound TGA and DTG is shown in Fig. 13. The TGA trace occurs at 154 °C and then decomposes into four phases. The first period of decomposition was between 154.8 °C and 255 °C and a weight loss of 46.76 percent. This would be attributed to the elimination of hydrogen, carbon and oxygen molecules from the material. Second level of decomposition

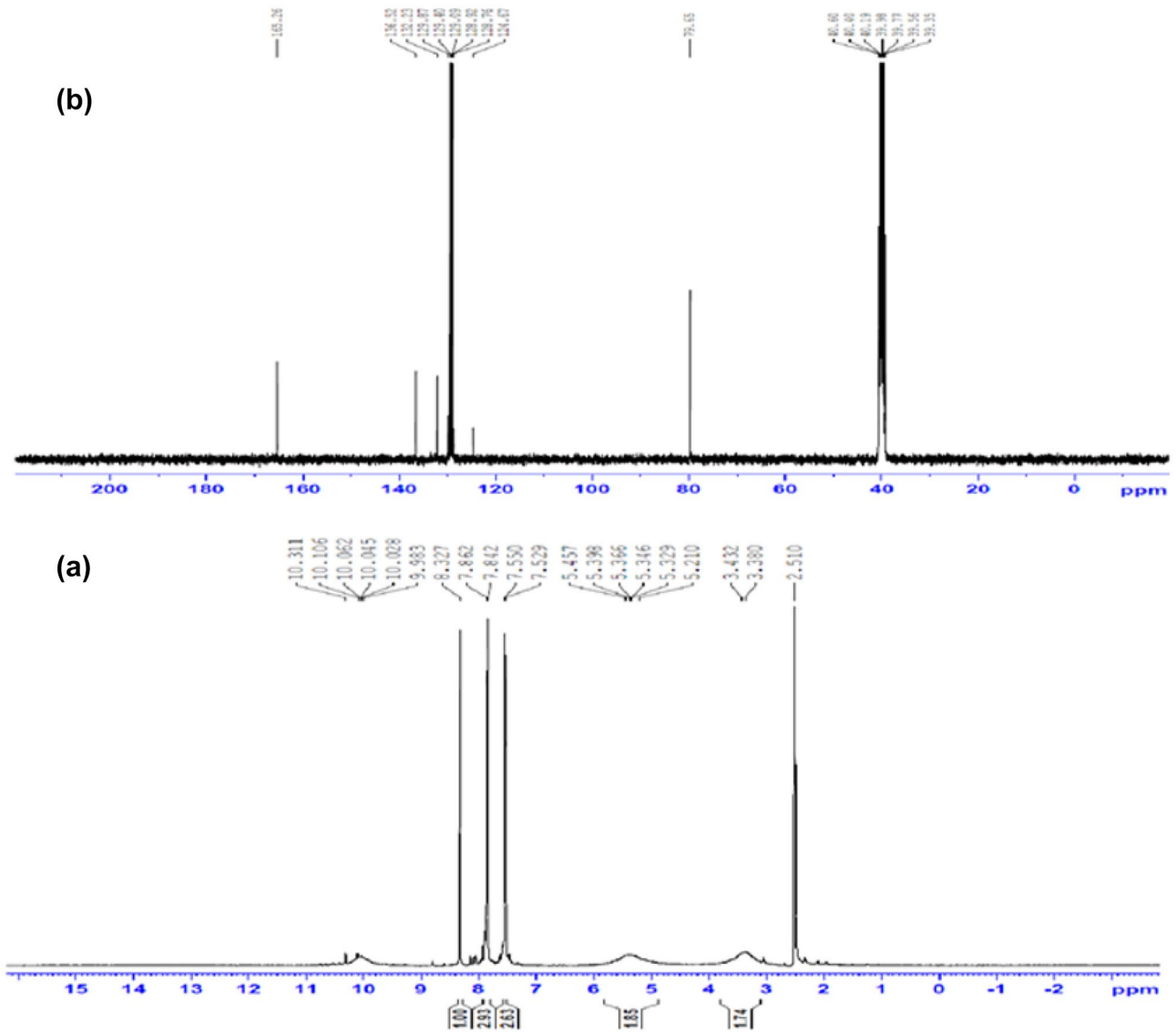

Fig. 9 1H and 13C NMR Spectrum of 4CBTCA single crystal

starts at 255.4 °C and ends at 324 °C with 18. 23% weight loss, which is owing to the removal of remaining carbon molecules, and two nitrogen groups. The third weight loss (31.61%) occurs between 255.8 °C and 350 °C, which prove that the decomposition is nearly complete. There is no weight loss between 351 °C and 450 °C due to the decomposition of the residue that is left over after the major weight loss, which corresponds to 2.29%. Differential scanning calorimetry analysis (DSC) is utilized for multitudinous applications in a wide range of industries, likewise involve glass transition and examinations of crystallization behaviour, melting and chemical reactions. Moreover, DSC applications assign with the impact of additives, fillers or the processing of materials. The DSC shows a very sharp exothermic peak at 143 °C which correlated to the melting of this compound, as presented in Fig. 14.

3.10 Third Order NLO Technique

The Z-scan measurement studied nonlinear characteristic properties of cultivated title crystal for nonlinear (β) and nonlinear refractive coefficients (n2). The Z-scan process is a common procedure that allows nonlinear optical properties of centrosymmetric crystals to be studied for the third order. It was a single system of experimental beam suggested by Prakash et. al. [46], with the goal of conducting and presenting information both on real and imaginary elements and on the sign of nonlinear and nonlinear material absorption. Figure 15(a) and (b) shows the amplitude recorded according to the distance between the opening and the closed curves. In order to calculate the absorption coefficient and nonlinear refraction index, the

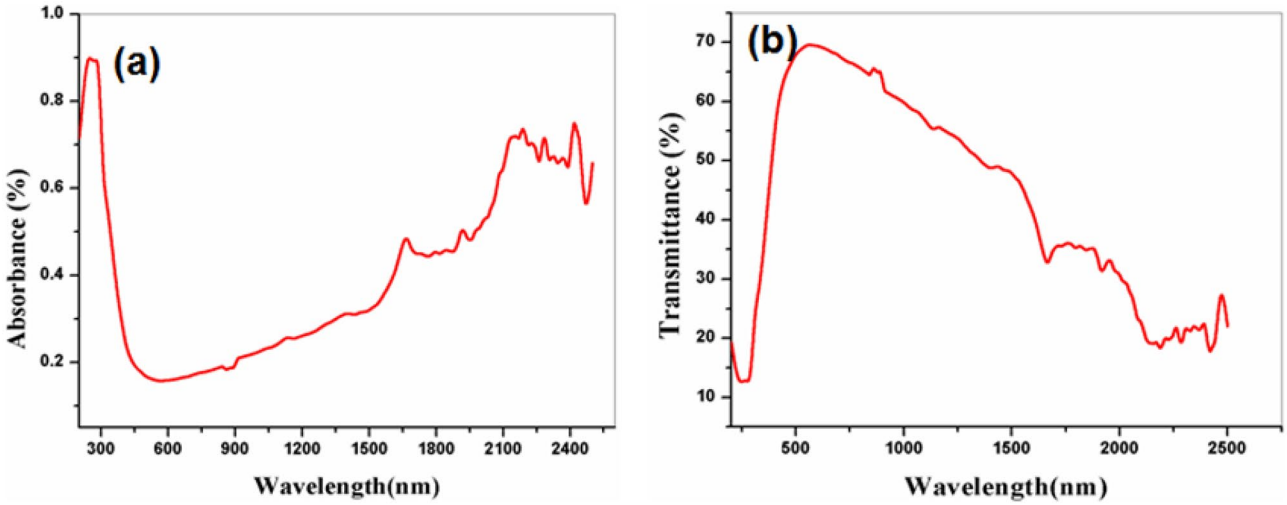

Fig. 10 Absorbance and transmittance spectrum of 4CBTCA single crystal

propagation of the sample from the far region by closed and open aperture modes permits the approximation of nonlinear refractive index and absorption coefficient. Since absorption coefficient and third-order nonlinear optical susceptibility are experimentally calculated by Z-scan method, these values are presented in Table 8. The closed aperture measurement followed by valley is owing to the self-defocusing nature of the title compound owing to local variation of refractive index [47]. In order that, we are finishing that the Z-scan experimental technique confirmed the third-order NLO properties. Sheik – Bahae et al. [48] have reported a single beam Z-Scan technique for the measurement of third-order nonlinear refractive index (n_2) and absorption coefficient (β) unitedly.

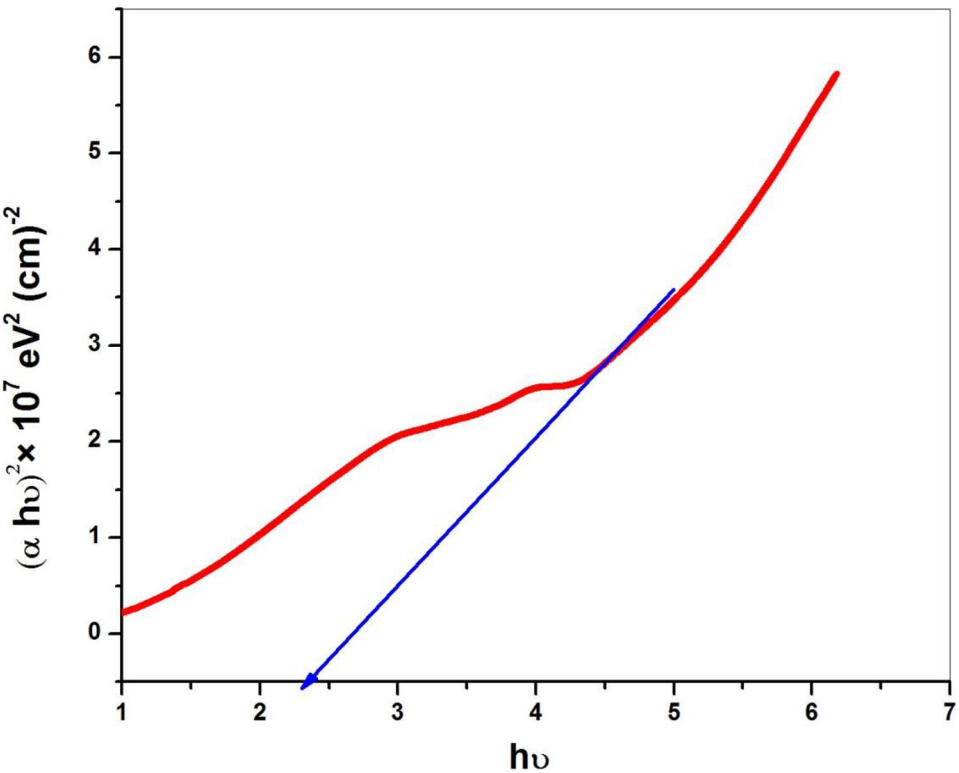

Fig. 11 Plot of (αhυ) 2 vs photon energy of 4CBTCA single crystal

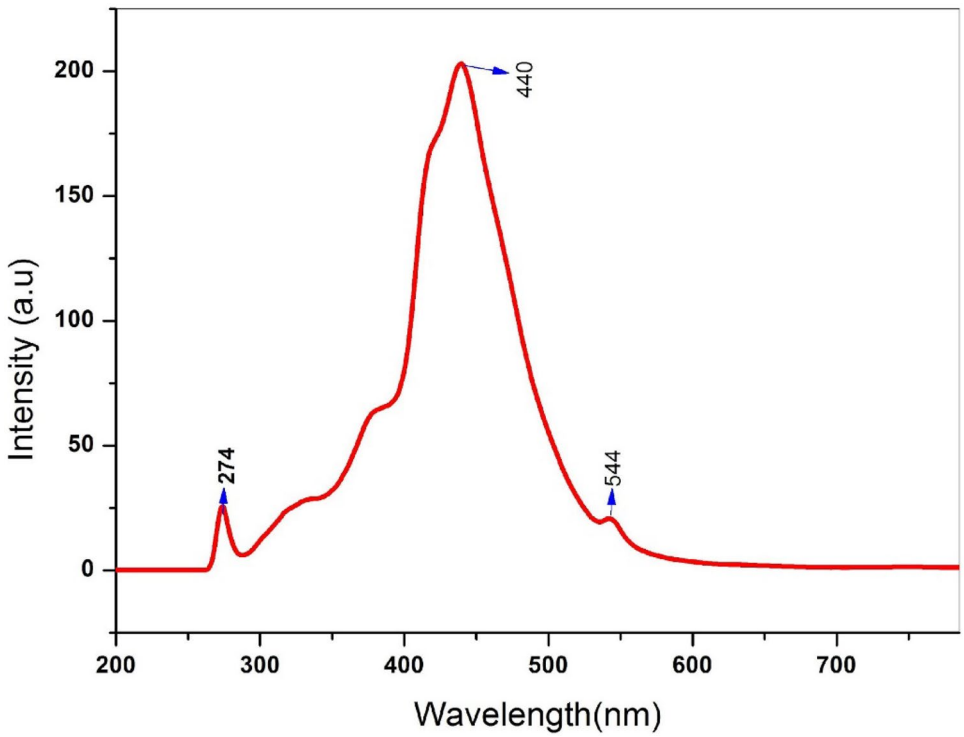

Fig. 12 Emission spectrum of 4CBTCA single crystal

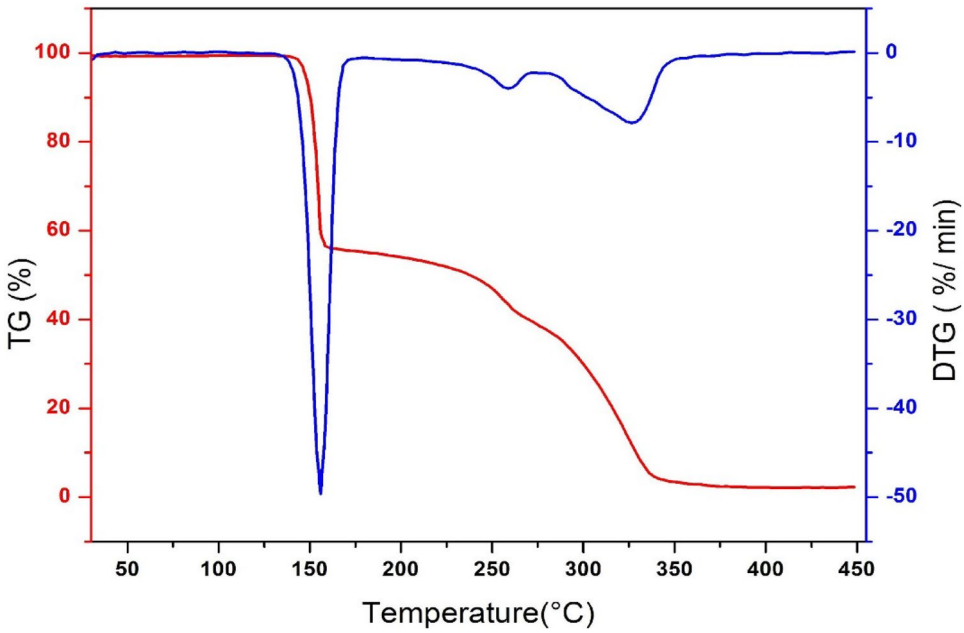

Fig. 13 TGA /DTA plots of 4CBTCA single crystal

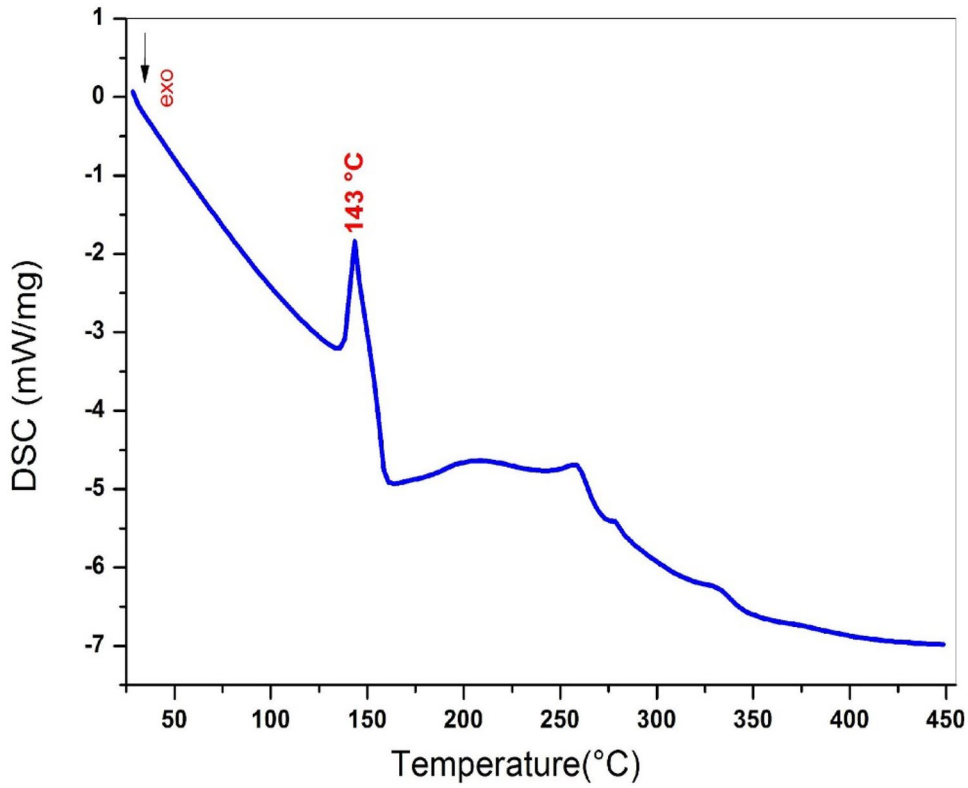

Fig. 14 DSC plots of 4CBTCA single crystal

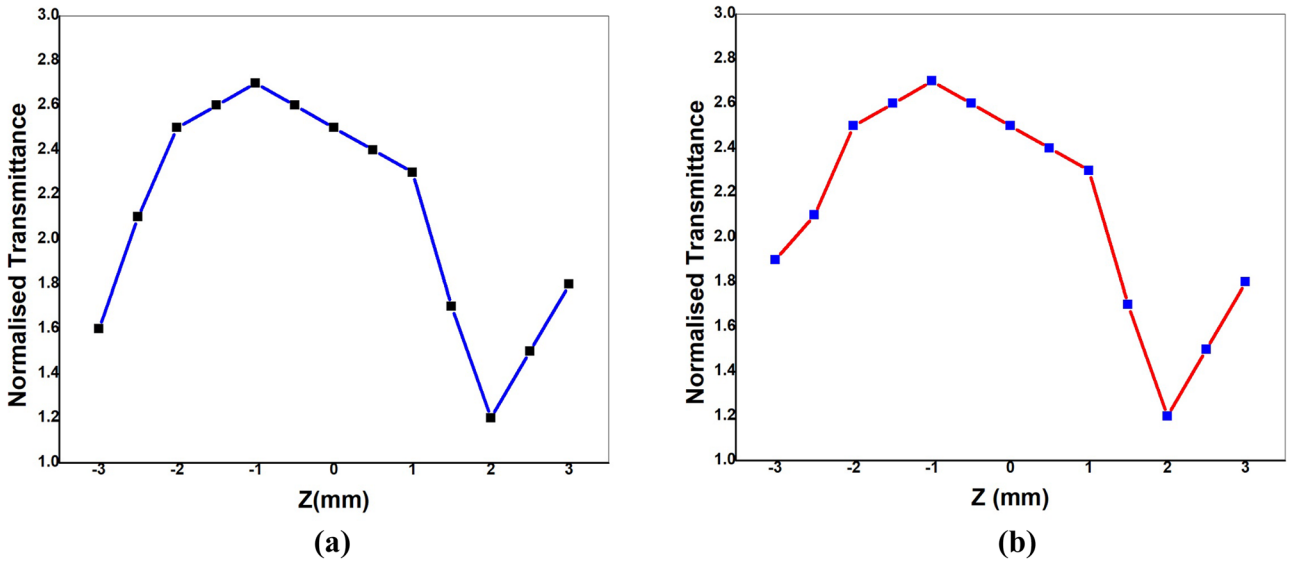

Fig. 15 (**a**) Z – scan (close) and (**b**) (open) spectrum of 4CBTCA

Table 8 Parameters measured in Z-scan experiment

Laser beam wavelength (λ)	632.8 nm
Lens focal length (f)	12 cm
Optical path distance (Z)	115 cm
Spot – size diameter in front of the aperture (ω_a)	1 cm
Aperture radius ($r_{a)}$	4 mm
Effective thickness (L_{eff})	0.99 mm
Nonlinear refractive index (n_2)	1.435×10^{-10} m^2/W
Nonlinear absorption coefficient (β)	0.3740×10^{-3} m/W
Real part of the third-order susceptibility [Re χ3]	5.77×10^{-8} cm2 W – 1
Imaginary part of the third-order susceptibility [Imχ3]	$2.2\ 1\times10^{-6}$ cm W – 1
Third order nonlinear susceptibility ($\chi^{(3)}$)	1.357×10^{-6} esu

4 Conclusions

Organic single crystal of 4-chlorobenzhydrazide trichloro acetate with a dimension $5\times3\times2$ mm^3 has been successfully grown by slow evaporation method. The 4CBTCA crystal was confirmed the triclinic crystal system with the centrosymmetric space group P $\bar{1}$ by single and powder X-ray diffraction studies. Ultraviolet–visible–near infrared analysis exhibits that 4CBTCA crystal is fully transparent throughout visible and near infrared region. The grown 4CBTCA single crystal has a huge spectrum of optical transmission and is suitable for optoelectronics applications. The structure and presence of various functional groups in the crystal were affirmed by NMR, FT-IR and FT-Raman studies, respectively. The fluorescence samples exhibit the green and blue emission of the 4CBTCA is a potential candidate for opto-electronic fluorescence applications. The thermal behaviour confirmed by the TGA and DTA. The third harmonic generation materials of 4CBTCA crystal were confirmed by the Z-scan method. The title compound promising structural, optical and thermal can be a potential materials for optoelectronics and frequency conversion devices and NLO optical limiting applications. The appearance of intermolecular interaction was revealed by Hirshfeld surface analysis.

Declarations

Conflict of Interest The authors declare that they have no known competing financial interests or personal relationships that could have appeared to influence the work reported in this paper.

References

1. S. Kumar, M.S. Niranjan, K.C. Chaluvaraju, C.M. Jamakhadi, Synthesis and biological evaluation of some sulfonamide schiff's bases. J. Curr. Pharm. Res. **1**, 39 – 42 (2010). https://www.researchgate.net/publication/44900173
2. S.Y. Mallikarjun, A.P. Sangamesh, Synthesis, evaluation of antioxidant activity and crystal structure of 2,4-dimethylbenzoylhydrazones. Trans. Met. Chem. **22**, 220–224 (1997). https://doi.org/10.3390/molecules180910912
3. A. Akelah , E.R. Kenawy, D.C. Sherrington, Agricultural polymers with herbicide/fertilizer function—III. Polyureas and poly(Schiff base)s based systems. J. Eur. Polym. **29**, 1041–1045 (1993). https://doi.org/10.1016/0014-3057(93)90306-Z
4. J.S. Jain, R.S. Srivastava, N. Aggarwal, R. Sinha, Synthesis and evaluation of schiff bases for anticonvulsant and behavioral depressant properties. Cent. Nerv. Syst. Agents Med. Chem. **7**, 200–204 (2007). https://doi.org/10.3390/molecules180910912
5. `G. Fareed, M.A. Versiani, N. Afza, N. Fareed, L. Iqbal, M. Lateef, Synthesis, spectroscopic characterization and pharmacological evaluation of oxazolone derivatives. J. Serb. Chem. Soc. **78**(8), 1127–1134 (2013). https://doi.org/10.2298/jsc120917126f
6. P. Mishra, P.N. Gupta, A.K. Shakya, R. Shukla, R.C. Srimal, Indian J. Physiol. Pharmacol **39**, 169–172 (1995)
7. C.T. Supuran, M. BarboiuLuca, C.E. Pop, M.E. Brewster, Carbonic anhydrase inhibitors. synthesis of topically effective intraocular pressure lowering agents derived from 5-(ω-aminoalkylcarboxamido)-1,3,4-thia-diazole-2- sulfonamide. Eur. J. Med. Chem. **31**, 597–606 (1996). https://doi.org/10.1080/14756369909030339
8. M.T. Tarafder, A. Kasbollah, N. Saravanan, K.A. Crouse, A.M. Ali, OoK, Syntheses, Characterization, In Vitro Antiglycation and DPPH Radical Scavenging Activities of Isatin Salicylhydrazide-hydr. Biochem. Mol. Bio. Biophy. **6**, 85–91 (2002). https://doi.org/10.1016/j.arabjc.2015.02.015
9. A. Walcourt, M. Loyevsky, D.B. Lovejoy, V.R. Gordeuk, D.R. Richardson, Novel aroylhydrazone and thiosemicarbazone iron chelators with anti-malarial activity against chloroquine-resistant and -sensitive parasites. Int. J. Biochem. Cell Biol. **36**, 401–407 (2004). https://doi.org/10.1016/s1357-2725(03)00248-6
10. M. Uthaya Kumar, A. Pricilla Jeyakumari, M. Suresh, S. Chandran, G. VinithaSynthesis, spectroscopic and DFT studies of Schiff based (E)-N'-(Benzo[d][1, 3]Dioxol-5-ylmethylene)nicotinohydrazide monohydrate single crystal: a promising organic nonlinear optical material. Mater. Res. Express **60**, 75102 (2019). https://doi.org/10.1088/2053-1591/ab13c7
11. P. Vicini, A. Geronikaki, M. Incerti, B. Busonera, G. Poni, C.A. Cabras, P.L. Colla, Synthesis and biological evaluation of benzo[d]isothiazole, benzothiazole and thiazole Schiff bases. Bioorg. Med. Chem. **11**(22), 4785–4789 (2003). https://doi.org/10.1016/s0968-0896(03)00493-0
12. A. Andreani, M. Rambaldi, D. Bonazzi, L. Greci, Andreani, Synthesis and cardiotonic activity of pyridylmethylene-24ndolinones. Sci. **34**, 132–138 (1979). https://doi.org/10.1016/0223-5234(92)90106-B

13. T. Suthan, N.P. Rajesh, C.K. Mahadevan, G. Bhagavannarayana, Studies on crystal growth and physical properties of 2-amino-5-chloropyridine single crystal. Mater. Chem. and Phy. **129**, 433–438 (2011). https://doi.org/10.1016/j.matchemphys.2011.04.038
14. S. Gaur, Synthesis, Characterization, Antimicrobial Activity, Antifungal Activity and DNA Cleavage Studies of Transition Metal Complexes with Schiff Base Ligand Asian. J. Chem. **15**, 250–254 (2003). https://doi.org/10.15680/IJIRSET.2015.0402010
15. M.J. Gemi, C. Biles, B.J. Keiser S.M. Poppe, S.M. Swaney, W.G. Tarapley, D.L. Romeso, Y. Yage. Novel 1,5-Diphenylpyrazole Nonnucleoside HIV-1 Reverse Transcriptase Inhibitors with Enhanced Activity versus the Delavirdine-Resistant P236L Mutant: Lead Identification and SAR of 3- and 4-Substituted Derivatives. Journal of Medicinal Chemistry, **43** (5), 1034–1040 (2000). https://doi.org/10.1021/jm990383f
16. A. Al-Amiery, Y.K. Al-Majedy, H.H. Ibrahim, Antioxidant, antimicrobial, and theoretical studies of the thiosemicarbazone derivative Schiff base 2-(2-imino-1-methylimidazolidin-4-ylidene)hydrazinecarbothioamide, Med. Chem. Lett. **2,** (2012) 2–4. https://orgmedchemlett.springeropen.com/track/pdf/10.1186/2191-2858-2-4
17. A.B. Corona, J.P. Viveros, A.P. Flores, A.C. Peraza, J.M. Martínez, M.M. Sumaya, R. Organillo, Antioxidant Activity of Butyl- and PhenylstannoxanesDerivedfrom 2-, 3- and 4-Pyridinecarboxylic Acids. Molecules **15** (8)**,** 5445–5459. https://doi.org/10.3390/molecules15085445
18. N. Dharmaraj, P. Viswanathamurthi, K. Natarajan, Ruthenium(II) complexes containing bidentateSchiff bases and their antifungal activity Trans. Met. Chem. **26**, 105–109 (2001). https://doi.org/10.1023/A:1007132408648
19. A. Özdemir, G. Turan-zitouni, Asimkaplancikli, Z., Demirci, F., &Iscan, G. Studies on hydrazone derivatives as antifungal agents. Journal of Enzyme Inhibition and Medicinal Chemistry, **23**(4),(2008) 470–475. https://doi.org/10.1080/14756360701709094
20. E. Maccioni, M.C. Cardia, L. Bonsignore, A. Plumitallo, M.L. Pellerano, A. De Logu, Synthesis and anti-microbial activity of isothiosemicarbazones and cyclic analogues. Il Farmaco **57**, 809–817 (2002)
21. S.G. Kuçukguzel, Biological Activities of Hydrazone Derivatives. Molecules, **12** (8), 1910–1939. 10.3390.
22. P.C. Lima, L.M. Lima, K.C. Silva, P.H. Leda, A.L.P Miranda C.A.M. Fraga, Barreiro, E.J. Lima, Synthesis and analgesic activity of novel N-acylarylhydrazones and isosters. Eur. J. Med. Chem. **35** (2), 187–203 (2000). https://doi.org/10.1016/s0223-5234(00)00120
23. J.L. Bredas, C. Adant, P. Tackx, A. Persoons, Mechanical, Dielectric and Photoconductivity Properties of L-Proline Succinate NLO Single Crystal. Chem. Rev. **94**, 243–278 (1994). https://doi.org/10.12691/jmpc-1-1-2
24. P.N. Prasad, D.J. Williams, Introduction to Nonlinear Optical Effects in Molecules and Polymers, John Wiley, (1991).
25. P. Audebert, K. Kamada, K. Matsunaga, K. Ohta, The third-order NLO properties of D-π-A molecules with changing a primary amino group into pyrrole. Chem. Phys. Lett. **367** (1–2), 62–71. https://doi.org/10.1016/s0009-2614(02)01575-0
26. K. Rajagopal, R.V. Krishnakumar, A. Mostad, S. Natarajan, L-Proliniumtrichloroacetate at 105 K. Acta. Crystallogr. E. Structure Reports Online. **59** (3), o277–o279. https://doi.org/10.1107/s1600536803002332
27. C. Arunagiri, A.G. Anitha, A. Subashini, S. Selvakumar, Synthesis, X-ray crystal structure, vibrational spectroscopy, DFT calculations, electronic properties and Hirshfeld analysis of (E) -4-Bromo- N '-(2,4-dihydroxy-benzylidene) benzohydrazide. J. Mol. Struct. **1163**, 368–378 (2018). https://doi.org/10.1016/j.molstruc.2018.03.023
28. K. Karthikeyan, I. Rama, A. Subashini, C. Arunagiri, S. Selvakumar, Crystal structure, hydrogen bonding, Hirshfeld surface analysis and inhibition efficiency of a Schiff base 2-methoxy-6-(naphthalene-2-yliminomethyl)-phenol. Chem. Data. Collect. **25**, (2020). https://doi.org/10.1016/j.cdc.2020.100337
29. C. Arunagiri, A. Subashini, M. Saranya, P. Thomas Muthiah, K. Thanigaimani, I. Abdul Razak. Spectrochim. Acta A Mol. Biomol. Spectrosc. **135**, 307- 316 (2015). https://doi.org/10.1016/j.saa.2014.07.016
30. A. Subashini, N.K. Lokanath, X–ray crystal structure, Hirshfeld surface analysis, DFT and electronic properties of (E)–4–chloro–N′–(2,4–dihydroxy–benzylidene) benzohydrazide. Chem. Data Collect. **19** (2018), 100174 (2019). https://doi.org/10.1016/j.cdc.2018.100174
31. J. Baran, A.J. Barnes, B. Engelen, M. Panthofer, A. Pietraszko, H. Ratajczak, M. Sledz, Structure and polarised IR and Raman spectra of the solid complex betaine–trichloroacetic acid. J. Mol. Struct. **55**, 21–41 (2000). https://doi.org/10.1016/s0022-2860(00)00381-1
32. P. V. Dhanaraj, N. P. Rajesh, G. Vinitha, G. Bhagavannarayana, Crystal structure and characterization of a novel organic optical crystal: 2-Aminopyridinium trichloroacetate. Mater. Res. Bull. **46** (5), 726–731 (2011). https://doi.org/10.1016/j.materresbull.2011.01.013
33. E. Selvakumar, A. Chandramohan, G. AnandhaBabu, P. Ramasamy, Synthesis, growth, structural, optical and thermal properties of a new organic salt crystal: 3-nitroanilinium trichloroacetate. J. Cryst. Growth **401**, 323–326 (2013). https://doi.org/10.1016/j.jcrysgro.2013.10.053
34. V. Crasta, V. Ravindrachary, S. Lakshmi, S.N. Pramod, M.A. Shridar, J.S. Prasad, Growth, characterization and crystal structure analysis of 1-(4-chlorophenyl)-3-(4-chlorophenyl) -2-propen-1-one, J. Cryst. Growth. **275**, 329 -335 (2005). https://doi.org/10.1016/j.jcrysgro.2004.10.110
35. M. Drozd, New complexes of guanidine with acetic, trichloroacetic and trifluoroacetic acids The DFT structural and vibrational investigationsSpectrochim. Acta Mol. Biomol. Spectrosc. **69**, 1223–1234 (2008). https://doi.org/10.1016/j.saa.2007.07.001
36. M.E. Peter, P. Ramasamy, Growth and characterization of an organic nonlinear optical crystal: Glyciniumtrichloroacetate-Mater. Chem. Phys. **137**, 258–263 (2012). https://doi.org/10.1016/j.matchemphys.2012.09.017
37. K. Karthikeyan, C. Arunagiri, A. Subashini, A.G. Anitha, Experimental and theoretical investigation of the molecular and electronic structure of 3 - acetoxy - 2- Methylbenzoic acid using Quantum Chemical computational Calculations. J. Chem. Pharm. Res. **9**, 262–280 (2017)
38. K. Karthikeyan, I. Rama, A. Subashini, C. Arunagiri, S. Selvakumar, Hydrogen bonding, Hirshfeld surface analysis and inhibation efficiency of a Schiff base 2 - methoxy - 6-(naphthalene - 2- yliminomethyl) - Phenol. Chem. Data collections, **25**, (2020) 100337
39. C. Arunagiri, A.G. Anitha, A. Subashini, S. Selvakumar, N.K. Lokanath, synthesis, single crystal, structure and Hirshfeld surface analysis of (E) - 4 - toluic - N - (2,4 - dihydroxy - benzylidene) benzohydrazide. Chem. Data. Collect. **17**, 169 - 177 (2018)
40. N.M. Ravindra, R.P. Bharadwaj, K. Sunil Kumar, V.K. Srivastava, Model based studies of some optical and electronic properties of narrow and wide gap materials. Infrared Phys. **21**, 369–381 (1981). https://doi.org/10.1016/0020-0891(81)90045-2
41. N.M. Ravindra, V.K. Srivastava, Electronic polarizability as a function of the penn gap in semiconductors. Infrared Phys. **20**, 67–69 (1980)
42. M.A. Spackman, D. Jayatilaka, Hirshfeld surface analysis. Cryst. Eng. Comm. **11**, 19–32 (2009)
43. M.A. Spackman, J.J. McKinnon, Fingerprinting intermolecular interactions in molecular crystals. Cryst. Eng. Comm. **4**, 378–392 (2002)

44. J.J. McKinnon, M.A. Spackman, A.S. Mitchell, Novel tools for visualizing and exploring intermolecular interactions in molecular crystals. Acta Cryst. B **60**, 627–668 (2004)
45. J.J. McKinnon, D. Jayatilaka, M.A. Spackman, Towards quantitative analysis of intermolecular interactions with Hirshfeld surfaces. Chem. Commun. **37**, 3814–3816 (2007)
46. M. Prakash, D. Geetha, M. Lydia Caroline, Crystal growth and characterization of L-phenylalaniniumtrichloroacetate—A new organic nonlinear optical material. Physica B: Condensed Matter. **406,** 2621-2625 (2011). https://doi.org/10.1016/j.physb.2011.04.002
47. M. Sheik – Bahae, A.A. Said, E.M. Van Stryland, Sensitive Measurement of Optical Nonlinearities Using a Single Beam. IEEE J. Quantum. Electron. **26**, 760 – 769 (1990)
48. M. Sheik – Bahae, A.A. Said, E.M. Van Stryland, High-sensitivity single-beam N2 measurements. Opt Lett. **14**, 955 – 957